Contemporary Mathematics
http://ojs.wiserpub.com/index.php/CM/

Research Article

A Delay-Embedded D-SIRS Model for Associated Credit Risk Contagion on Complex Networks: Threshold, Equilibrium, and Robustness Analysis

Xiaogang Liu[1,3], Jinmian Han[1,2], Yue Lei[3], Dongqi Yue[1], Huaigu Tian[3*]

[1] School of Economics and Management, Northwest University, Xi'an 710127, China
[2] Research Institute of Economy and Development of Western China, Northwest University, Xi'an 710127, China
[3] Xi'an Key Laboratory of Human-Machine Integration and Control Technology for Intelligent Rehabilitation, Xijing University, Xi'an 710123, China
E-mail: tianhuaigu@foxmail.com

Received: 10 March 2026; **Revised:** 14 May 2026; **Accepted:** 25 May 2026

Abstract: Associated credit risk can propagate through inter-firm credit, trade, asset, and liquidity linkages, particularly when risk recognition and intervention are delayed. Here we develop a delay-embedded delay-embedded susceptible-infected-recovered-susceptible (D-SIRS) model to study credit-risk contagion on complex inter-firm networks. The model combines a degree-based mean-field framework with degree-dependent asset connectedness, allowing network structure and exposure heterogeneity to jointly shape the contagion mechanism. We derive the contagion threshold and identify the conditions under which local credit stress either dies out or becomes persistent. The threshold rises with stronger immunization and recovery, but falls with longer delays, stronger asset connectedness, faster immunity waning, and greater degree heterogeneity. Numerical simulations show that Barabási-Albert (BA) scale-free networks have lower stability boundaries than more homogeneous benchmark networks. Node-level Monte Carlo simulations further show that the threshold-type transition remains visible under stochastic finite-network propagation, while robustness checks show that concentrating asset connectedness among high-degree firms amplifies systemic vulnerability. These results suggest that associated credit-risk governance should combine preventive screening, timely intervention, and post-distress recovery, rather than rely on a single policy instrument.

***Keywords*:** associated credit risk contagion, delay-embedded D-SIRS model, degree-based mean-field framework, network heterogeneity, contagion threshold

MSC: 91G45, 91G40, 05C82

1. Introduction

Inter-firm credit risk contagion has become a central issue in modern financial risk management as firms, banks, suppliers, and investors are connected through credit, trade, asset, liquidity, and supply-chain linkages. Recent episodes in regional banking, global shipping networks, and leveraged cross-market positions show that financial stress is rarely confined to a single institution or market segment. Local shocks may travel through contractual exposures, funding dependence, trade-credit chains, and balance-sheet connections, and delayed responses can allow stress to accumulate

Copyright ©2026 Huaigu Tian, et al.
DOI: https://doi.org/10.37256/cm.7420269876
This is an open-access article distributed under a CC BY license
(Creative Commons Attribution 4.0 International License)
https://creativecommons.org/licenses/by/4.0/

before effective identification or intervention takes place. This view is consistent with production-network research showing that microeconomic shocks can propagate through input-output linkages and generate aggregate fluctuations, with the strength of propagation depending on network structure [1]. Evidence from the Great East Japan Earthquake also shows that supply-chain disruptions can generate large and persistent economic effects [2], while recent work on supply-chain disruptions further emphasizes the macroeconomic consequences of delayed adjustment in interconnected production systems [3]. These observations highlight the importance of understanding how inter-firm associated credit risk, namely credit risk transmitted through trade-credit, asset-exposure, and supply-chain relationships, propagates across economic networks.

The early foundations of financial risk contagion research can be traced back to Allen and Gale [4], who showed that risk can spread through financial linkages among entities. Cifuentes et al. [5] further examined the role of liquidity risk in cross-market transmission and demonstrated that liquidity risk and credit-market failures are important contagion channels. Gai and Kapadia [6] demonstrated that contagion in financial networks may arise through direct and indirect connections and may display nonlinear threshold effects. Elliott et al. [7] emphasized that the failure of key nodes can trigger systemic risk, while Acemoglu et al. [8] analyzed how network topology shapes financial stability. Tipsri and Chinviriyasit [9] showed from a transmission-dynamics perspective that delay effects can influence contagion processes and intensify crisis diffusion. Luo and Tan [10] further examined risk contagion in international short-term capital flows and found that volatility spillovers may increase risks to global financial stability. These studies provide an important theoretical foundation for analyzing financial contagion. However, this literature mainly clarifies contagion channels, systemic amplification, and network-based instability. The joint role of network heterogeneity, delayed response, and inter-firm asset connectedness remains less fully developed within a unified dynamic threshold framework.

Complex network theory provides a structural basis for studying such propagation. Watts and Strogatz [11], Barabási and Albert [12], and Newman [13] show that real networks often display clustering, short paths, and heterogeneous degree distributions. In financial and economic networks, these structural properties imply that a small number of highly connected nodes may have disproportionate influence on shock transmission. Buldyrev et al. [14] highlighted that failures in interdependent networks may generate cascading collapse. Haldane and May [15] argued that financial networks may improve risk sharing under normal conditions but become fragile when connections are dense and strongly coupled. Glasserman and Young [16] further emphasized that contagion depends not only on network structure, but also on transmission channels and feedback effects. Taken together, this literature shows that topology is central to systemic risk. Yet topology alone does not specify how delayed recognition, recovery, immunity waning, and exposure heterogeneity jointly alter the contagion threshold and the long-run risk regime.

Epidemic dynamics models such as susceptible-infected-susceptible (SIS), susceptible-infected-recovered (SIR), and susceptible-exposed-infected-recovere (SEIR) provide useful tools for analyzing contagion thresholds, dynamic paths, and equilibrium states. Ma et al. [17], Liu et al. [18], and Sun and Liu [19] extended epidemic models to examine the effects of delay, threshold conditions, and network heterogeneity on transmission processes. Liu [20] analyzed a delayed SEIR model and documented that delays may cause instability and intensify contagion. These studies provide tractable methods for modeling dynamic propagation. However, when epidemic models are applied to financial risk, the economic meaning of states, parameters, and transition mechanisms must be made explicit. In particular, inter-firm credit contagion requires a clear mapping from epidemiological states to financial conditions, from network degree to firm connectedness, and from transmission intensity to direct asset exposure.

A related strand of literature focuses on systemic risk measurement and financial connectedness. DebtRank [21], connectedness measures based on variance decompositions [22], network connectedness indicators [23], and financial-network composition analysis [24] have improved the identification of risk linkages and system-wide exposure. Zhao et al. [25] analyzed multidimensional and multilayer extreme-risk transmission in China's banking sector and emphasized the importance of internal and external interconnections as well as delay effects. Baruník et al. [26] examined the persistence of financial connectedness, while Camera and Gioffré [27] studied financial contagion and financial lockdowns.

This strand of research strengthens the empirical and measurement foundation for systemic-risk analysis. Empirical connectedness studies provide useful tools for identifying risk linkages and measuring systemic exposure, but they often focus on observed connectedness patterns rather than on the analytical threshold through which delay, exposure

heterogeneity, and governance capacity jointly determine the persistence of contagion. In the context of inter-firm associated credit risk, such a unified threshold framework remains insufficiently developed.

Despite the rich literature on financial contagion, complex networks, epidemic dynamics, and systemic-risk measurement, three important gaps remain in the dynamic modeling of inter-firm associated credit risk. First, delay mechanisms remain insufficiently incorporated into models of inter-firm credit contagion. Delays in risk identification, information reporting, and intervention may affect not only the speed of contagion, but also the contagion threshold, the steady-state risk level, and the marginal effects of governance strategies. Second, network heterogeneity is often simplified. Existing models frequently capture the number of connections but pay less attention to how direct asset connectedness varies across firms with different degrees. This may understate the role of highly connected firms that also carry stronger asset exposures. Third, the dynamic effects of risk-prevention and risk-resolution mechanisms are not fully integrated. Existing studies often examine single measures or static comparisons, making it difficult to evaluate the complementarity, substitution, and diminishing marginal effects of ex ante immunization and ex post recovery under different network structures and delay conditions. These gaps are not merely technical. Even when existing approaches adequately describe current credit-risk conditions, they may still underestimate how delays, heterogeneous asset connectedness, and incomplete governance responses accelerate stress accumulation and narrow the effective window for timely intervention.

To address these gaps, we develop a delay-embedded D-SIRS model to analyze inter-firm associated credit-risk contagion on complex networks. The model integrates delayed risk recognition, degree-based network heterogeneity, and governance through immunization and recovery within a unified threshold framework. This structure allows us to examine how slower identification and intervention alter the stability boundary, how degree-dependent asset connectedness amplifies the systemic role of highly connected firms, and how prevention and recovery jointly affect long-run risk regimes. We derive the contagion threshold, distinguish between risk-free and endemic-risk steady states, and validate the mechanism through numerical simulations, node-level Monte Carlo analysis, and robustness checks. The results clarify when local credit shocks become persistent and how coordinated governance can raise the resilience of the associated credit network.

The remainder of this paper is organized as follows. Section 2 presents the inter-firm credit network, model assumptions, and delay-embedded D-SIRS formulation. Section 3 derives the contagion threshold and analyzes the equilibrium structure. Section 4 reports the numerical analysis of threshold sensitivity, delay effects, network size, and steady-state outcomes. Section 5 provides node-level Monte Carlo validation and robustness checks. Section 6 concludes with the main findings, policy implications, and limitations.

2. Research design

2.1 *Associated credit network and model assumptions*

Consider an associated credit network with N firms. Nodes represent firms, and edges represent direct asset or transaction linkages, including guarantees, accounts receivable and payable relationships, cross-shareholding, and capital transactions. Let k denote firm degree. For firms in degree class k, the direct asset connectedness ratio measures the share of directly linked assets in total assets.

The contagion process follows an SIRS-type structure. Firms without realized credit distress are in the susceptible state $S(t)$. Firms experiencing default, credit-rating deterioration, liquidity stress, or expanding risk exposure enter the infected state $I(t)$ and become sources of contagion. Through operational adjustment, external financing, regulatory intervention, trade-credit support, or credit extension, infected firms may move into the immunized state $R(t)$, where their short-term probability of reinfection is reduced. Because risk exposure, recognition, intervention, and recovery do not occur instantaneously, the delay parameter T is introduced to capture the system-level response lag. Immunity is temporary: protection may decay, or new shocks may return immunized firms to the susceptible state. Susceptible firms may also enter the immunized state directly through ex ante risk screening, exposure reduction, or early-warning intervention. This cyclic structure allows local credit stress either to die out or to become persistent within the network.

Based on this setting, the model is built on the following assumptions.

Hypothesis 1 Firms are classified into three credit-risk states: susceptible firms S, infected firms I, and immunized firms R. Susceptible firms have not yet experienced credit-risk distress but may be exposed to external shocks or contagion through asset and transaction linkages. Infected firms have experienced default, credit deterioration, liquidity stress, or a significant expansion of risk exposure. Immunized firms have stronger short-term resistance because of internal adjustment, external support, or effective risk-mitigation measures.

Hypothesis 2 The baseline network is closed over the relevant contagion horizon. The number of firms remains fixed, and firm entry and exit are not explicitly modelled. This assumption is appropriate for short- to medium-run analysis in which the main concern is distress propagation among existing credit relationships rather than network formation or firm demography. It does not imply that bankruptcy, exit, or crisis-induced network rewiring is unimportant. Rather, these events define the boundary of the baseline model. If firm replacement or network restructuring becomes large enough to alter the degree distribution or exposure matrix, the threshold condition should be re-evaluated under a time-varying network.

Hypothesis 3 The baseline model assumes a common delay structure across firms. The delay captures the average lag between risk exposure, risk identification, information response, and effective intervention. It should therefore be interpreted as a system-level response lag, not as a claim that all firms respond identically. Heterogeneous delay structures are left for future extensions.

Before introducing degree-dependent asset connectedness, it is important to distinguish connection quantity from exposure intensity. Firm degree k captures the number of direct linkages, whereas the direct asset connectedness ratio captures the asset-exposure intensity associated with those linkages. A highly connected firm may therefore be systemically important not only because it has more counterparties, but also because its balance sheet is more strongly tied to them.

Hypothesis 4 Inter-firm association is heterogeneous. For firms with degree k, η_k denotes the average direct asset connectedness ratio of degree class k, defined as the share of directly linked assets in total assets, with $0 < \eta_k < 1$. Higher-degree firms may also have stronger asset connectedness, but η_k is treated as a degree-dependent exposure parameter rather than as a constant.

These assumptions define the analytical boundary of the model. They do not attempt to capture all features of dynamically evolving credit networks. Instead, they allow the paper to derive a clear contagion threshold and to identify how delay, network heterogeneity, asset connectedness, immunization, recovery, and immunity waning jointly shape the stability boundary. Alternative network sizes and degree-dependent asset connectedness are examined in the numerical and robustness analyses, while heterogeneous delays and time-varying networks are reserved for future research.

This specification implies that the exposure term entering the contagion threshold is degree-weighted. The constant-exposure case, $\eta_k = \eta_0$ for all k, is used only as a benchmark in the numerical analysis.

Table 1 reports the key network quantities and model parameters. These variables define the structure of the delay-embedded D-SIRS framework and link the theoretical model to the financial interpretation of associated credit risk.

Table 1. Key network quantities and parameters in the delay-embedded D-SIRS model

Symbol	Definition	Role in the model
N	Number of firms in the associated credit network	Defines the finite network scale used in threshold and robustness analysis
$k, P(k)$	Firm degree and degree distribution	Capture network connectivity and heterogeneity across firms
$\langle k \rangle, \langle k^2 \rangle$	First and second degree moments	Determine the structural effect of network heterogeneity on the contagion threshold
$S_k(t), R_k(t)$	Densities of susceptible and immunized firms with degree k at time t	Describe vulnerable and protected firms within each degree class
$I_{k,\tau}(t)$	Density of infected firms with degree k at delay stage τ	Captures infected firms that remain active during the delay process
$I_k(t)$	Total infected density of firms with degree k	Aggregates delay-stage infected densities within each degree class
$\theta(t)$	Probability that a randomly selected link points to an infected firm	Measures edge-weighted exposure to infected counterparties
η_k	Degree-dependent direct asset connectedness ratio	Captures exposure heterogeneity across degree classes

Table 1. (cont.)

Symbol	Definition	Role in the model
η_0	Constant-exposure benchmark value of direct asset connectedness	Used only when $\eta_k = \eta_0$ for all k in the benchmark simulations
β	Baseline contagion intensity	Determines whether credit risk can cross the contagion threshold
δ	Immunity waning rate	Captures the loss of protection and return from the immunized state to the susceptible state
α	Ex ante immunization rate	Represents preventive risk screening, exposure reduction, or early-warning intervention
γ	Ex post recovery rate	Represents recovery, restructuring, liquidity support, or post-distress resolution
T	Contagion delay length	Captures lags in risk identification, information disclosure, intervention, or recovery

Notes: η_k is degree dependent. The constant-exposure benchmark, $\eta_k = \eta_0$ for all k, is used only in the numerical simulations. The contagion threshold and the degree-weighted asset-connectedness term are defined in Section 3

Although the model is not calibrated to a specific historical episode, its core variables have direct empirical counterparts. Firm degree k can be constructed from observed inter-firm credit, guarantee, trade-credit, receivable-payable, or transaction linkages. The degree-dependent asset connectedness ratio η_k can be measured by the share of related receivables, guarantees, cross-shareholdings, capital transactions, or other direct inter-firm exposures in total assets within each degree class. The delay length T can be proxied by lags in risk identification, reporting, disclosure, intervention, or recovery. The immunization rate α corresponds to ex ante screening, early-warning coverage, exposure reduction, or preventive credit control, while the recovery rate γ captures debt restructuring, liquidity support, guarantee resolution, or post-distress recovery capacity. These mappings clarify how the theoretical framework could be calibrated in future research using firm-level linkage, balance-sheet exposure, or transaction data.

2.2 *Delay-embedded D-SIRS model*

Building on delayed epidemic models showing that response lags can reshape stability, threshold conditions, and long-run transmission outcomes [28, 29], we formulate a delay-embedded D-SIRS model under a degree-based mean-field framework. Firms are grouped by degree class rather than treated as identical agents. The state variables therefore describe the average dynamics within each degree group, while the model retains the threshold-relevant effects of the degree distribution $P(k)$, degree moments, edge-weighted contagion probability $\theta(t)$, and degree-dependent direct asset connectedness η_k. This closure preserves network and exposure heterogeneity at the degree-class level, while abstracting from realization-specific edge configurations for analytical tractability. Section 5.1 complements this analytical framework with node-level Monte Carlo simulations on finite BA networks. The delay-embedded D-SIRS model is specified as follows:

$$\begin{cases} \frac{dS_k(t)}{dt} = -\eta_k \beta k \theta S_k(t) + \delta R_k(t) - \alpha S_k(t) \\ \frac{dI_{k,0}(t)}{dt} = \eta_k \beta k \theta S_k(t) - \gamma I_{k,0}(t) \\ \frac{dI_{k,1}(t)}{dt} = \gamma I_{k,0}(t) - \gamma I_{k,1}(t) \\ \vdots \\ \frac{dI_{k,T}(t)}{dt} = \gamma I_{k,T-1}(t) - \gamma I_{k,T}(t) \\ \frac{dR_k(t)}{dt} = \gamma I_{k,T}(t) + \alpha S_k(t) - \delta R_k(t) \end{cases} \tag{1}$$

The delay mechanism is represented by a chain of infected compartments. This formulation captures the fact that credit stress is not identified, processed, resolved, or absorbed instantaneously. Once a firm enters the infected state, its

distress remains active over a sequence of delay stages before recovery and immunization take effect. The $T+1$ infected compartments in System (1) therefore provide a tractable representation of delayed risk absorption while preserving the degree-based network structure.

Here, $I_{k,\tau}(t)$ denotes the density of infected firms with degree k at delay stage τ, where $\tau = 0, 1, \cdots, T$. The total infected density of firms in degree class k is

$$I_k(t) = \sum_{\tau=0}^{T} I_{k,\tau}(t). \tag{2}$$

Let $\theta(t)$ denote the probability that a randomly selected edge points to an infected firm at time t. Under the degree-based mean-field framework, this edge-weighted contagion probability is

$$\theta(t) = \frac{1}{\langle k \rangle} \sum_k kP(k)I_k(t), \langle k \rangle = \sum_k kP(k). \tag{3}$$

Thus, $\theta(t)$ is an edge-weighted measure of infection pressure rather than a simple average infected density. The weight $kP(k)/\langle k \rangle$ assigns greater influence to high-degree infected firms, reflecting their stronger capacity to transmit credit stress through multiple counterparties. This treatment keeps the threshold-relevant role of network heterogeneity within the mean-field structure.

The aggregate densities of susceptible, infected, and immunized firms are

$$S(t) = \sum_k P(k)S_k(t), I(t) = \sum_k P(k)I_k(t), R(t) = \sum_k P(k)R_k(t). \tag{4}$$

System (1) nests several benchmark specifications under suitable parameter restrictions, including models without ex ante immunization, without immunity waning, or without contagion delay.

3. Threshold and equilibrium analysis

3.1 *Equilibrium states and contagion threshold*

We characterize the long-run regimes of System (1) through its steady states. This focus is consistent with delayed epidemic models in which response lags can alter stability boundaries and long-run transmission outcomes [30]. Let S_k^*, I_k^*, and R_k^* denote the steady-state densities in degree class k, and let S^*, I^*, and R^* denote the corresponding aggregate steady-state densities. The system admits two economically distinct regimes: a risk-free steady state and an endemic-risk steady state.

Definition 1 If the infected density converges to zero, the system is in a risk-free steady state. If the infected density converges to a positive constant, the system is in an endemic-risk steady state.

Definition 2 Let β denote the contagion intensity of associated credit risk. The critical value β_c is defined as the contagion threshold. When $\beta < \beta_c$, local credit stress cannot sustain persistent propagation in the associated credit network.

Theorem 1 Define the degree-weighted asset-connectedness term as

$$M_\eta = \sum_k k^2 P(k)\eta_k. \tag{5}$$

Under the delay-embedded D-SIRS model, the contagion threshold is

$$\beta_c = \frac{< k > \gamma(\delta + \alpha)}{\delta(T+1)M_\eta}. \tag{6}$$

If $\beta < \beta_c$, the risk-free equilibrium is locally stable and associated credit risk cannot generate persistent contagion. If $\beta > \beta_c$, the risk-free equilibrium loses local stability, and a nontrivial endemic-risk steady state may emerge.

Proof. At the steady state, the delay-chain equations imply

$$I^*_{k,0} = I^*_{k,1} = \cdots = I^*_{k,T}.$$

Since

$$I^*_k = \sum_{\tau=0}^{T} I^*_{k,\tau},$$

we have $I^*_{k,T} = \frac{I^*_k}{T+1}$.

Using the steady-state conditions of the infection and recovery equations, the total infected density in degree class k can be written as

$$I^*_k = \frac{\eta_k \beta k \theta (T+1)\delta}{\gamma(\delta+\alpha) + \eta_k \beta k \theta (\delta(T+1)+\gamma)}.$$

The edge-weighted probability that a randomly selected link points to an infected firm is

$$\theta^* = \frac{1}{\langle k \rangle} \sum_k k P(k) I^*_k.$$

Substituting I^*_k into this expression yields the self-consistency equation

$$\theta^* = \frac{1}{\langle k \rangle} \sum_k k P(k) \frac{\eta_k \beta k \theta^* (T+1)\delta}{\gamma(\delta+\alpha) + \eta_k \beta k \theta^* (\delta(T+1)+\gamma)} = f(\theta^*).$$

The trivial solution $\theta^* = 0$ corresponds to the risk-free equilibrium. A positive solution emerges when the slope of $f(\theta^*)$ at $\theta^* = 0$ exceeds one. The threshold condition is therefore given by $f'(0) = 1$. Since

$$f'(0) = \frac{\delta \beta (T+1) M_\eta}{\gamma(\delta+\alpha)\langle k \rangle},$$

the threshold condition gives

$$\beta_c = \frac{\langle k \rangle \gamma(\delta + \alpha)}{\delta(T+1)M_\eta}.$$

This threshold should therefore be interpreted as a local stability boundary under the degree-based mean-field closure. It should not be read as a global stability result for every finite-network realization. □

Remark 1 Degree-dependent asset connectedness.

In the general model, η_k is a degree-class-specific asset-exposure parameter. It therefore enters the threshold through the weighted term M_η, not as a scalar outside the summation. The constant-exposure case, $\eta_k = \eta_0$ for all k, is used only as a benchmark in the numerical analysis. Because the weight in M_η is proportional to $k^2 P(k)$, increases in asset connectedness among high-degree firms have a stronger threshold effect than equivalent increases among low-degree firms.

Corollary 1 Constant-exposure and homogeneous-network benchmarks.

If direct asset connectedness is constant across degree classes, that is, $\eta_k = \eta_0$ for all k, then

$$M_\eta = \eta_0 \langle k^2 \rangle .$$

The threshold in Eq. (6) reduces to

$$\beta_c^0 = \frac{\langle k \rangle \gamma}{\langle k^2 \rangle (T+1)\eta_0} \left(1 + \frac{\alpha}{\delta}\right). \tag{7}$$

If the network is homogeneous and the degree distribution is highly concentrated, so that $\langle k^2 \rangle \approx \langle k \rangle^2$, the threshold further becomes

$$\beta_c^{\text{hom}} = \frac{\langle k \rangle \gamma(\delta + \alpha)}{\langle k^2 \rangle \delta(T+1)\eta_0} = \frac{\gamma}{\langle k \rangle (T+1)\eta_0} \left(1 + \frac{\alpha}{\delta}\right). \tag{8}$$

Corollary 1 shows that, under the constant-exposure benchmark, network heterogeneity affects the stability boundary through the structural ratio $\langle k \rangle / \langle k \rangle$. A larger second-degree moment lowers the contagion threshold and makes persistent risk propagation easier to sustain.

Corollary 2 No-delay benchmark and the threshold-reducing effect of delay.

If the contagion delay is not considered, that is, $T = 0$, the threshold becomes

$$\beta_c(0) = \frac{\langle k \rangle \gamma(\delta + \alpha)}{\delta M_\eta} = \frac{\langle k \rangle \gamma}{M_\eta} \left(1 + \frac{\alpha}{\delta}\right).$$

With delay, the threshold is

$$\beta_c(T) = \frac{\langle k \rangle \gamma(\delta + \alpha)}{\delta(T+1)M_\eta} = \frac{\langle k \rangle \gamma}{M_\eta(T+1)} \left(1 + \frac{\alpha}{\delta}\right).$$

Hence,

$$\beta_c(0) = (T+1)\beta_c(T) > \beta_c(T), \text{for } T > 0. \tag{9}$$

Corollary 2 implies that ignoring delay overstates the stability boundary and may understate the vulnerability of the associated credit network. Economically, longer lags in risk recognition, information disclosure, intervention, or recovery allow credit stress to remain active for more stages before being absorbed, thereby lowering the threshold for persistent contagion.

Theorem 1 identifies the stability boundary linking network topology, exposure heterogeneity, delay, and governance capacity. The term M_η combines degree heterogeneity and asset-exposure heterogeneity in a single threshold-relevant measure. A larger M_η indicates stronger asset connectedness in degree-weighted terms, especially when highly connected firms also carry larger direct asset exposures. This lowers the contagion threshold and increases systemic vulnerability. By contrast, stronger immunization α and recovery γ raise the threshold, while longer delay T and faster immunity waning δ reduce it. The result shows how local credit shocks become persistent when network structure, exposure concentration, and delayed governance jointly weaken the system's stability boundary.

Economically, M_η captures the interaction between network centrality and asset-exposure concentration. A larger M_η lowers the stability boundary, particularly when high-degree firms also carry large direct asset linkages. Stronger immunization and recovery raise this boundary, whereas longer delays and faster immunity waning reduce it. Persistent contagion is therefore most likely when exposure concentration and delayed governance amplify the fragility created by network heterogeneity.

3.2 *Threshold sensitivity and BA scale-free network case*

Starting from the general threshold in Eq. (6), we examine how governance capacity, delay, and degree-weighted asset connectedness shape the stability boundary of the associated credit network. For the sensitivity analysis, T is interpreted through its continuous relaxation. The comparative-static derivatives are

$$\begin{aligned}
\frac{\partial \beta_c}{\partial \gamma} &= \frac{\langle k \rangle (\delta + \alpha)}{\delta (T+1) M_\eta} > 0, \\
\frac{\partial \beta_c}{\partial \alpha} &= \frac{\langle k \rangle \gamma}{\delta (T+1) M_\eta} > 0, \\
\frac{\partial \beta_c}{\partial T} &= -\frac{\langle k \rangle \gamma (\delta + \alpha)}{\delta M_\eta (T+1)^2} < 0, \\
\frac{\partial \beta_c}{\partial M_\eta} &= -\frac{\langle k \rangle \gamma (\delta + \alpha)}{\delta (T+1) M_\eta^2} < 0, \\
\frac{\partial \beta_c}{\partial \delta} &= -\frac{\langle k \rangle \gamma \alpha}{(T+1) M_\eta \delta^2} < 0.
\end{aligned} \tag{10}$$

The comparative statics identify two opposing forces in the stability boundary. Stronger recovery γ and ex ante immunization α raise the contagion threshold, making persistent risk propagation harder to sustain. Longer delay T works in the opposite direction because credit stress remains active for more stages before being absorbed. Faster immunity waning δ also lowers the threshold when $\alpha > 0$, as protected firms return more quickly to the susceptible state. The

negative derivative with respect to M_η shows that stronger degree-weighted asset connectedness reduces the stability boundary and increases systemic vulnerability.

Since M_η aggregates asset connectedness across degree classes, the marginal effect of exposure intensity should be evaluated at the degree-class level. For a given degree class j,

$$M_\eta = \sum_k k^2 P(k)\eta_k, \text{ we have } \frac{\partial M_\eta}{\partial \eta_j} = j^2 P(j).$$

Therefore,

$$\frac{\partial \beta_c}{\partial \eta_j} = -\frac{\langle k \rangle \gamma(\delta+\alpha) j^2 P(j)}{\delta(T+1)M_\eta^2} < 0. \tag{11}$$

Equation (11) shows that an increase in direct asset connectedness lowers the contagion threshold in every degree class. Its marginal effect, however, is weighted by $j^2 P(j)$. The same increase in exposure intensity therefore has a larger threshold-reducing effect when it occurs among highly connected firms. This result provides a theoretical basis for the systemic role of core firms in associated credit networks: they transmit stress through more counterparties, and when their direct asset linkages are also stronger, local credit shocks are more likely to cross the systemic contagion threshold.

This emphasis on degree heterogeneity is consistent with epidemic spreading on heterogeneous networks, where thresholds depend critically on degree moments and the influence of highly connected nodes [31]. To link the general threshold condition to a finite heterogeneous network, we consider the finite-size BA scale-free benchmark. Since the associated credit network contains a finite number of firms, the degree distribution is evaluated over the support $k \in [m, k_{\max}(N)]$. To avoid applying the asymptotic power-law form directly to a finite network without normalization, we use the normalized finite-size BA degree distribution

$$P_{BA,N}(k) = \frac{k^{-3}}{\sum_{j=m}^{k_{\max}(N)} j^{-3}},\ k = m, \cdots, k_{\max}(N). \tag{12}$$

The corresponding first and second degree moments are

$$\langle k \rangle_{BA,N} = \sum_{k=m}^{k_{\max}(N)} k P_{BA,N}(k),\ \langle k^2 \rangle_{BA,N} = \sum_{k=m}^{k_{\max}(N)} k^2 P_{BA,N}(k). \tag{13}$$

These finite-size moments capture average connectivity and degree heterogeneity in the BA benchmark. When asset connectedness is degree dependent, however, the exposure term entering the threshold is not determined by $\langle k^2 \rangle_{BA,N}$ alone. It is given by

$$M_{\eta,N}^{BA} = \sum_{k=m}^{k_{\max}(N)} k^2 P_{BA,N}(k)\eta_k. \tag{14}$$

Substituting Eq. (14) into the general threshold condition gives the finite-size BA threshold:

$$\beta_c^{BA}(N) = \frac{\langle k \rangle_{BA,N} \gamma(\delta + \alpha)}{\delta(T+1) M_{\eta,N}^{BA}}, \tag{15}$$

Equation (15) shows that the BA-network threshold is shaped jointly by finite-size degree heterogeneity and degree-dependent asset connectedness. This formulation is consistent with a finite firm network and avoids reducing η_k to a scalar exposure factor outside the summation.

Under the constant-exposure benchmark, $\eta_k = \eta_0$ for all k, we have

$$M_{\eta,N}^{BA} = \eta_0 \sum_{k=m}^{k_{\max}(N)} k^2 P_{BA,N}(k) = \eta_0 \langle k^2 \rangle_{BA,N}.$$

The finite-size BA threshold then reduces to

$$\beta_c^{BA,0}(N) = \frac{\langle k \rangle_{BA,N} \gamma(\delta + \alpha)}{\delta(T+1) \eta_0 \langle k^2 \rangle_{BA,N}}. \tag{16}$$

This benchmark expression is used in the baseline numerical simulations. If η_k increases with k, high-degree firms receive larger exposure weights in $M_{\eta,N}^{BA}$, which lowers $\beta_c^{BA}(N)$ relative to the constant-exposure benchmark. BA scale-free networks are therefore especially vulnerable when degree concentration and asset-exposure concentration coincide. In financial terms, core firms become more systemically important not only because they are connected to more counterparties, but also because stronger direct asset linkages make local shocks more likely to cross the systemic contagion threshold.

4. Numerical analysis

4.1 *Benchmark setting and cross-network threshold comparison*

This section uses numerical simulations to illustrate the contagion threshold mechanism derived in Section 3. The simulations are designed not to reproduce a specific historical episode but to examine systematically how network topology, governance parameters, direct asset connectedness, and contagion delay jointly shape the stability boundary of the associated credit network. This mechanism-oriented approach provides a consistent basis for comparing threshold effects across network structures.

The benchmark network comprises $N = 1000$ nodes, sufficiently large to capture meaningful degree heterogeneity while remaining computationally tractable. Three canonical network structures are considered: a BA scale-free network, where each new node attaches with $m = 5$ links, yielding an average degree $\langle k \rangle \approx 10$ and producing a heterogeneous network with high-degree hubs; a WS small-world network, in which each node is initially connected to $K = 2m = 10$ nearest neighbors and a rewiring probability $p_{WS} = 0.05$ introduces limited long-range links while preserving clustering and a concentrated degree distribution; and an exponential network, with a degree-decay parameter $\varepsilon = 2$, generating an intermediate degree distribution between the BA and WS benchmarks. For the BA and exponential networks, finite-size normalized degree distributions are used. The average degree is kept broadly comparable across networks, ensuring that differences in the contagion threshold primarily reflect degree heterogeneity rather than network density. Network-size robustness is examined in Section 5.3.

The baseline financial and governance parameters are set as follows: $\alpha = 0.20$, $\gamma = 0.30$, $\eta_0 = 0.30$, $\delta = 0.10$, and $T = 5$. These values are not intended to reproduce a specific historical episode. They define an interior moderate-risk regime in which prevention, recovery, asset connectedness, immunity waning, and delay are all active. Specifically, α represents a moderate level of ex ante immunization through risk screening, exposure control, or early-warning intervention;

γ reflects a moderate post-distress recovery capacity; η_0 is used as the benchmark direct asset connectedness ratio under the constant-exposure specification; δ captures gradual immunity waning after temporary stabilization; and T denotes a finite recognition-and-response delay rather than a specific calendar lag. This setting allows the threshold effects of each mechanism to be compared without forcing the system into immediate extinction or nearly automatic persistence. Subsequent sensitivity and robustness analyses examine whether the main mechanism remains robust to changes in these parameters, network size, and degree-dependent asset connectedness.

In this subsection, the constant-exposure benchmark is used, namely $\eta_k = \eta_0$ for all degree classes. The contagion threshold is therefore computed according to the constant-exposure threshold in Eq. (7). The degree-dependent specification of η_k is examined later in the robustness analysis. Accordingly, η_0 in Figure 1 should be interpreted as the benchmark direct asset connectedness ratio, rather than as a general degree-dependent exposure parameter.

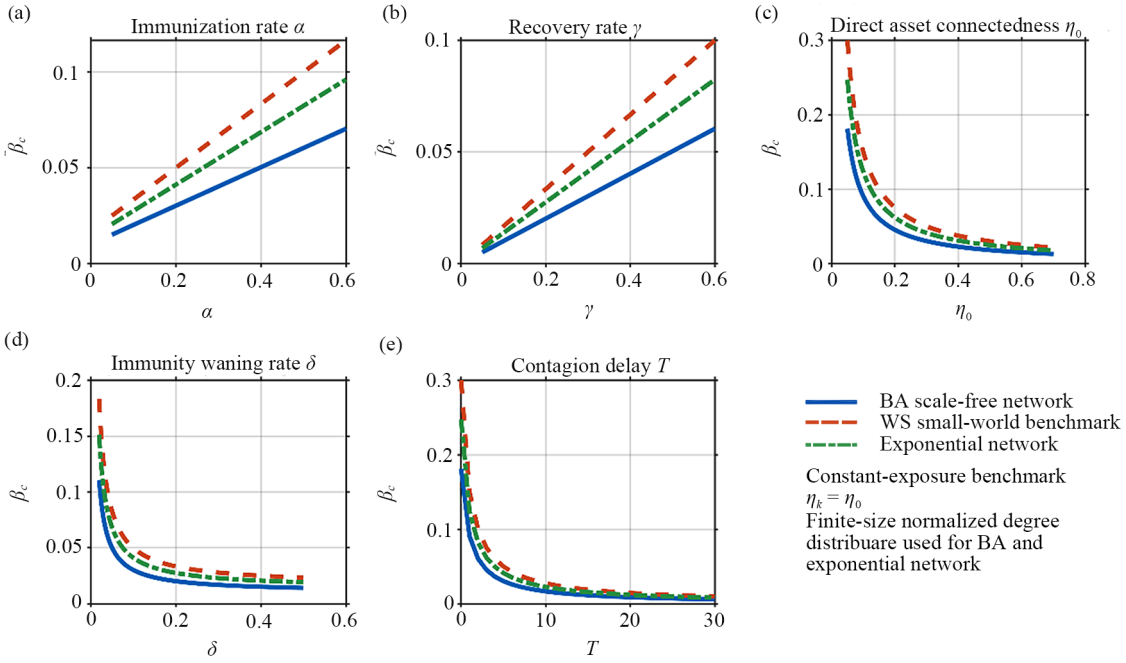


Figure 1. Parameter effects on the contagion threshold across network structures. The figure reports the contagion threshold β_c for the BA scale-free network, WS small-world benchmark, and exponential network under the constant-exposure benchmark $\eta_k = \eta_0$. Figure 1a–e vary α, γ, η_0, δ, and T, respectively, with all other parameters fixed at their benchmark values. The BA and exponential networks are computed using finite-size normalized degree distributions

Figure 1 compares how key parameters affect the contagion threshold β_c under the BA scale-free network, Watts-Strogatz (WS) small-world benchmark, and exponential network. The figure reports threshold-level comparative statics rather than full contagion dynamics. Dynamic paths, steady-state infection levels, and node-level simulation validation are examined in later sections.

Figure 1a,b show that the contagion threshold increases with the immunization rate α and the recovery rate γ. This pattern is consistent with the comparative-static results in Section 3.2. Economically, stronger ex ante immunization moves vulnerable firms into a protected state before risk materializes, while a higher recovery rate improves ex post resolution and reduces the persistence of infected firms. Both mechanisms expand the stability boundary of the associated credit network.

Figure 1c shows that the threshold decreases as the benchmark direct asset connectedness ratio η_0 increases. Under the constant-exposure benchmark, a higher η_0 strengthens the asset-linkage channel through which local credit shocks are transmitted. This lowers the critical threshold for sustained contagion. In the general degree-dependent case, the corresponding effect is captured by the degree-weighted exposure term M_η, rather than by a scalar exposure parameter.

Figure 1d,e show that the threshold declines with the immunity waning rate δ and the contagion delay T. A larger δ means that the protective effect of prior immunization or recovery decays more quickly, allowing firms to re-enter the susceptible state sooner. A longer T reflects slower risk identification, information disclosure, or intervention, which gives credit risk more time to accumulate and transmit. Both effects compress the stability boundary and make persistent contagion more likely.

The cross-network comparison further shows that the BA scale-free network generally has the lowest threshold across the parameter ranges. Under the constant-exposure benchmark, network structure affects the threshold mainly through the structural ratio $\langle k\rangle/\langle k^2\rangle$, computed from the corresponding degree distribution of each network. For the finite-size BA benchmark, this ratio is $\langle k\rangle_{BA,N}/\langle k^2\rangle_{BA,N}$. The BA network has stronger degree heterogeneity and a larger second-degree moment, $\langle k^2\rangle_{BA,N}$, which lowers the threshold. The WS benchmark, with a more concentrated degree structure, tends to have a higher threshold. The exponential network usually lies between these two cases, depending on the degree-decay parameter. These results indicate that stronger network heterogeneity reduces the contagion threshold and increases structural vulnerability.

Overall, Figure 1 provides a benchmark setting in which governance capacity, asset connectedness, immunity waning, delay, and network heterogeneity can be compared through their effects on the contagion threshold.

4.2 *Effects of contagion delay and network size*

This subsection examines how contagion delay and network size affect the contagion threshold under the finite-size BA scale-free network. The analysis uses the constant-exposure benchmark, $\eta_k = \eta_0$ for all degree classes, so that the effects of delay length T and network size N can be isolated from degree-dependent exposure heterogeneity.

To avoid numerical artifacts that may arise from applying an asymptotic degree distribution directly to a finite network, the normalized finite-size BA degree distribution is recalculated for each value of N. The corresponding first and second degree moments, $\langle k\rangle_{BA,N}$ and $\langle k^2\rangle_{BA,N}$, are then recomputed before the contagion threshold is evaluated. This procedure ensures that the reported network-size effect reflects changes in finite-size degree heterogeneity rather than a plotting or normalization artifact.

The governance and exposure parameters are held at their benchmark values from Section 4.1. The network size varies from $N = 500$ to $N = 5000$, and the delay length T takes integer values over the reported range. Very small network sizes are excluded because the finite-size BA degree distribution is not a meaningful approximation to a macro-level inter-firm network near the lower boundary of N. If such very small N values are included, the threshold may display a sharp local increase. This increase reflects a finite-size boundary effect caused by the strongly truncated degree distribution and the resulting high value of $\langle k\rangle_{BA,N}/\langle k^2\rangle_{BA,N}$. It should therefore not be interpreted as a separate economic mechanism.

Figure 2 reports the joint and separate effects of contagion delay and network size on the contagion threshold. Figure 2a shows the joint effect of N and T in the finite-size BA network. The threshold is higher when the delay is short and the network is relatively small. As T increases, the threshold declines, indicating that longer risk-recognition or intervention delays reduce the stability boundary of the associated credit network.

Figure 2b isolates the delay effect at selected network sizes. For each reported network size, the threshold decreases as T increases. This pattern is consistent with the threshold expression, in which the delay term enters through $T + 1$. Economically, a longer delay allows credit stress to remain active for more stages before recovery takes effect. As a result, a lower contagion intensity may be sufficient to sustain propagation.

Figure 2c focuses on the network-size effect under selected positive delay levels. The no-delay case, $T = 0$, is retained as a theoretical benchmark in Figure 2b, but the positive-delay cases are emphasized in Figure 2c because they correspond more directly to delayed risk recognition and intervention. The declining pattern indicates that larger finite-size BA networks have lower contagion thresholds under otherwise identical governance and exposure conditions.

Figure 2d provides the structural explanation for this result. The structural ratio $\langle k\rangle_{BA,N}/\langle k^2\rangle_{BA,N}$ declines as N increases. Since the threshold under the constant-exposure benchmark is proportional to this ratio, a lower $\langle k\rangle_{BA,N}/\langle k^2\rangle_{BA,N}$ directly translates into a lower contagion threshold. This pattern reflects the increasing role of degree heterogeneity in larger finite-size BA networks.

The apparent threshold spike that may occur near very small network sizes should be interpreted as a finite-size boundary effect. It is caused by the strong truncation of the degree distribution near the lower boundary of N, which can temporarily raise $\langle k\rangle_{BA,N}/\langle k^2\rangle_{BA,N}$. It is therefore not a separate economic mechanism. By restricting the reported range to $N = 500$–5000 and recalculating the finite-size BA degree distribution and its moments for each N, Figure 2 focuses on the relevant finite-network size effect rather than on a small-network artifact.

Figure 2 therefore shows that contagion delay and network size jointly compress the stability boundary of the associated credit network. Longer delay lowers the threshold through a temporal persistence channel, while larger finite-size BA networks lower the threshold through a structural heterogeneity channel. This result is consistent with the finite-size BA threshold expression.

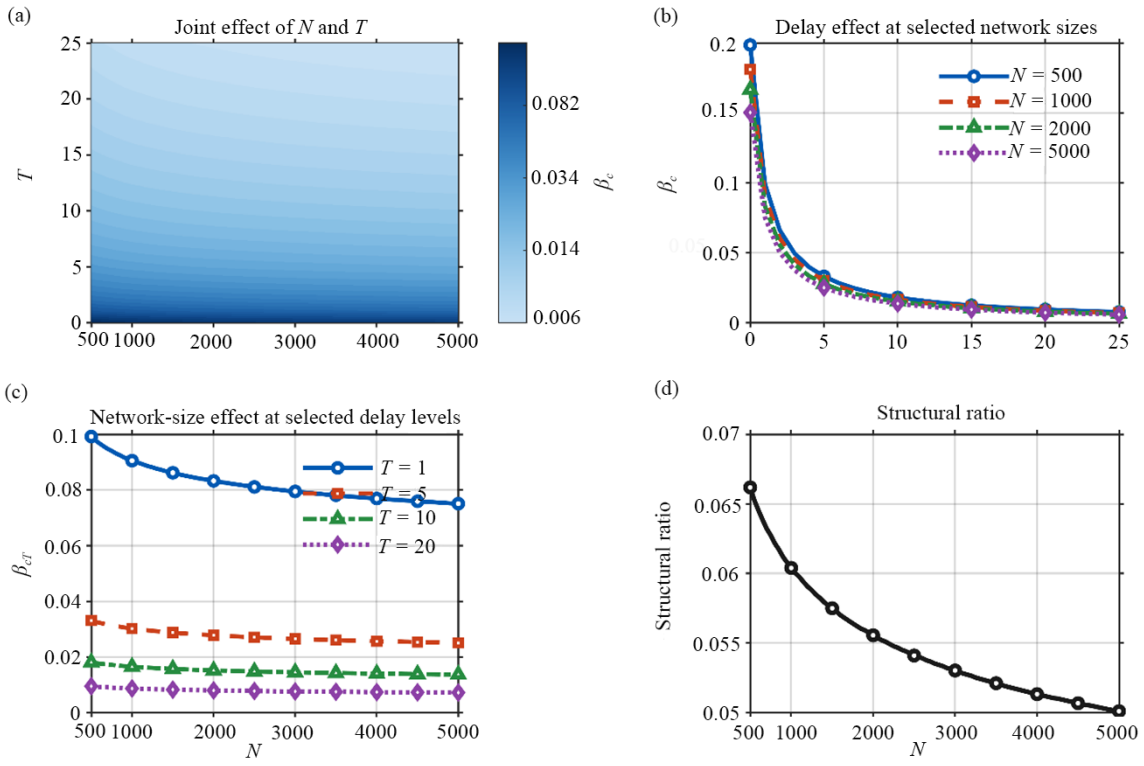


Figure 2. Effects of contagion delay and network size on the contagion threshold under the finite-size BA network.The figure reports the contagion threshold under the constant-exposure benchmark, $\eta_k = \eta_0$ for all degree classes. Figure 2a presents the joint effect of network size N and contagion delay T in the $N - T$ plane over the range $N = 500$ to $N = 5000$. A log-scaled color map is used only for visual clarity, while the colorbar reports the original threshold values. Figure 2b shows the delay effect at selected network sizes. Figure 2c shows the network-size effect at selected positive delay levels. Figure 2d plots the structural ratio $\langle k\rangle_{BA,N}/\langle k^2\rangle_{BA,N}$. For each value of N, the normalized finite-size BA degree distribution and the corresponding degree moments are recalculated before the threshold is computed

4.3 *Dynamic evolution and steady-state outcomes*

After examining the threshold effects of network structure, contagion delay, and network size, this subsection turns to the dynamic evolution of firm-state densities and the formation of steady-state infection outcomes. The purpose is to show how the threshold mechanism is reflected in the time paths of susceptible, infected, and immunized firms, and how long-run infection levels are formed under the finite-size BA network.

The dynamic trajectories are obtained by numerically integrating the delay-embedded D-SIRS system in System (1). For consistency with the benchmark analysis in Sections 4.1 and 4.2, the main simulations continue to use the constant-exposure benchmark, $\eta_k = \eta_0$. This setting keeps the focus on the dynamic implications of the threshold mechanism, while the degree-dependent specification of η_k is examined later in the robustness analysis.

The steady-state infected density is computed from the degree-based mean-field fixed point rather than imposed through an aggregate closed-form approximation. Specifically, the fixed point θ^* is obtained from the self-consistency equation. Given θ^*, the degree-specific infected density I_k^* is calculated for each degree class. The aggregate steady-state infected density under the finite-size BA network is then obtained by averaging I_k^* over the finite-size BA degree distribution. This procedure keeps the steady-state calculation consistent with both the degree-based mean-field framework and the finite-size BA specification used in the threshold analysis.

For the dynamic simulation, the network, governance, and exposure parameters follow the benchmark setting used above. The finite-size BA network and the constant-exposure benchmark $\eta_k = \eta_0$ are maintained. The contagion intensity is not chosen arbitrarily; instead, it is set to $\beta = 1.5\beta_c^{BA,0}(N)$, so that the system lies above the benchmark finite-size BA threshold and admits a positive steady-state infected density.

The initial condition is $S(0) = 0.95$, $I(0) = 0.05$, and $R(0) = 0$, representing a small initial credit-risk shock.

Figure 3 shows how the system evolves once the contagion intensity exceeds the finite-size BA threshold. Figure 3a reports the aggregate densities of susceptible, infected, and immunized firms. Starting from a small initial shock, the infected density first increases, indicating that credit risk propagates through the associated network. It then declines gradually as recovery and immunization mechanisms take effect. However, the infected density does not converge to zero. Instead, it approaches a positive long-run level, which is consistent with the existence of an endemic-risk steady state when $\beta > \beta_c^{BA,0}(N)$.

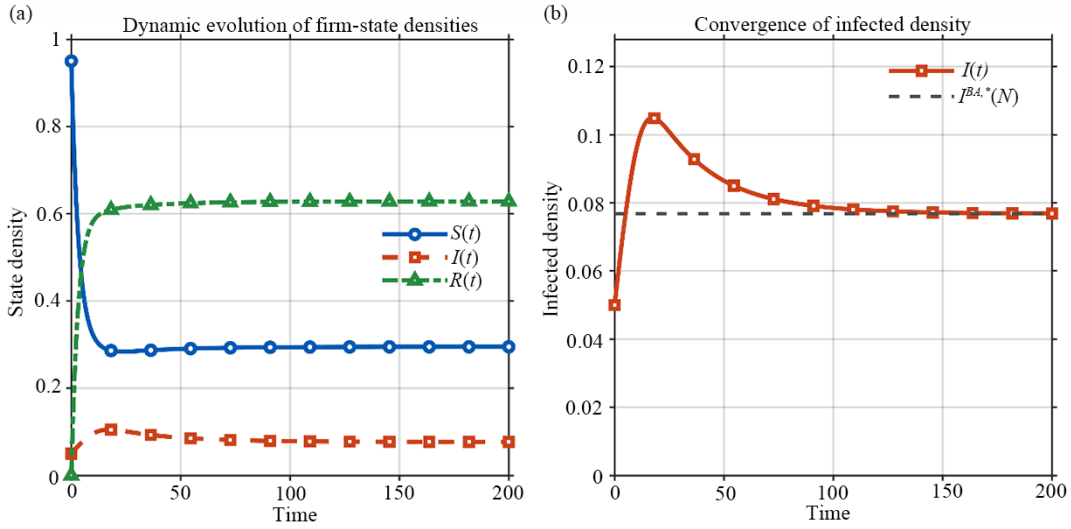


Figure 3. Dynamic evolution and steady-state infected density under the finite-size BA network. The figure reports the dynamic evolution of aggregate susceptible, infected, and immunized firm densities under the finite-size BA network. The simulation uses the constant-exposure benchmark $\eta_k = \eta_0$ and sets the contagion intensity to $\beta = 1.5\beta_c^{BA,0}(N)$, placing the system above the benchmark finite-size BA threshold. Figure 3a shows the time paths of $S(t)$, $I(t)$, and $R(t)$. Figure 3b compares the simulated infected density with the steady-state infected density $I^{BA,*}(N)$ computed from the degree-based mean-field fixed point

The susceptible and immunized densities adjust in opposite directions during the early stage of contagion. The susceptible density falls quickly as firms either become exposed to risk transmission or move into the immunized state. The immunized density rises and then stabilizes, reflecting the role of ex ante protection and post-contagion recovery in absorbing part of the risk pressure. In this model, $R(t)$ should be interpreted as an immunized or protected state, rather than only as a conventional recovery outcome.

Figure 3b focuses on the infected density and compares the simulated path with the steady-state infected density computed from the degree-based mean-field fixed point. The simulated $I(t)$ initially exceeds its long-run level and then converges toward $I^{BA,*}(N)$. This convergence indicates that the numerical integration of System (1) is consistent with the

fixed-point calculation of the steady-state infected density. It also confirms that, under the benchmark supercritical setting, the system does not return to the risk-free state but settles at a positive infection level.

Figure 3 complements the threshold analysis in Figures 1 and 2. The threshold results show when persistent contagion becomes possible, while Figure 3 illustrates how the system moves toward a nonzero steady-state infection level once the threshold is crossed. This dynamic pattern supports the interpretation that the finite-size BA network can sustain long-run credit-risk propagation when contagion intensity exceeds the stability boundary.

The steady-state infected density used in the following simulations is computed from the degree-based mean-field fixed point. For firms with degree k, the steady-state infected density is

$$I_k^* = \frac{\delta \eta_k \beta k \theta^* (T+1)}{\gamma(\delta+\alpha) + \eta_k \beta k \theta^* [\delta(T+1)+\gamma]}. \tag{17}$$

Under the finite-size BA network, the aggregate steady-state infected density is obtained by averaging I_k^* over the normalized finite-size BA degree distribution $P_{BA,N}(k)$:

$$I^{BA*}(N) = \sum_{k=m}^{k_{\max}(N)} P_{BA,N}(k) I_k^* . \tag{18}$$

The fixed point θ^* is determined by the corresponding mean-field self-consistency equation:

$$\theta^* = \frac{1}{\langle k \rangle_{BA,N}} \sum_{k=m}^{k_{\max}(N)} k P_{BA,N}(k) \frac{\delta \eta_k \beta k \theta^* (T+1)}{\gamma(\delta+\alpha) + \eta_k \beta k \theta^* [\delta(T+1)+\gamma]}. \tag{19}$$

When the contagion intensity is below the corresponding threshold, the fixed point collapses to $\theta^* = 0$, and the aggregate steady-state infected density is zero. When a positive fixed point exists, Eq. (18) gives the long-run infected density under the finite-size BA network. In the baseline numerical simulations, we use the constant-exposure benchmark $\eta_k = \eta_0$ for all degree classes. The degree-dependent specification of η_k is examined separately in the robustness analysis.

After confirming that the dynamic path converges to the degree-based mean-field steady state, we further examine how contagion delay affects the long-run infected density. Unlike Figure 2, which focuses on the contagion threshold β_c, Figure 4 reports the steady-state infected density $I^{BA,*}(N)$ computed from the finite-size BA fixed point. The contagion intensity is set relative to the reference threshold $\beta_c^{ref} = \beta_c^{BA,0}(N, T=5)$, which allows the effect of delay to be evaluated under comparable contagion-intensity settings.

Figure 4 reports the effect of contagion delay on the steady-state infected density $I^{BA,*}(N)$ under the finite-size BA fixed-point framework. Figure 4a shows the result under the baseline contagion intensity $\beta = 1.5\beta_c^{ref}$. For short delay lengths, the steady-state infected density remains zero because the fixed contagion intensity is still below the corresponding delay-specific threshold. As T increases, the threshold declines, and the same contagion intensity becomes sufficient to generate a positive endemic-risk steady state. The steady-state infected density then rises with the delay length.

Figure 4b compares this delay effect under different contagion intensities. For a given delay length, a larger β leads to a higher $I^{BA,*}(N)$. The curves also show that longer delay allows more contagion-intensity settings to cross the threshold and sustain positive infection levels. This pattern is consistent with the threshold result in Figure 2 and the dynamic convergence result in Figure 3.

Figure 4 shows that contagion delay affects not only the timing of propagation but also the long-run infection outcome. Longer delay lowers the stability boundary and increases the steady-state infected density once the system enters the supercritical region. This result suggests that delayed risk recognition, information disclosure, or intervention can increase the persistence of credit-risk contagion under the finite-size BA network.

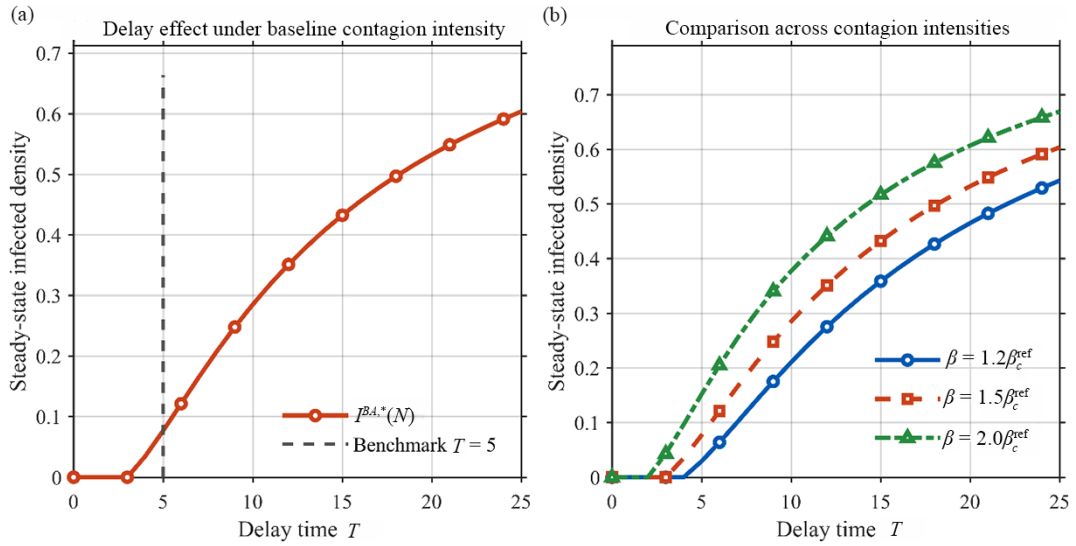


Figure 4. Effects of contagion delay on steady-state infected density under the finite-size BA network. The figure reports the steady-state infected density $I^{BA,*}(N)$ computed from the degree-based mean-field fixed point under the finite-size BA network. The simulation uses the constant-exposure benchmark $\eta_k = \eta_0$. The contagion intensity is set relative to the reference threshold $\beta_c^{ref} = \beta_c^{BA,0}(N, T = 5)$. Figure 4a shows the delay effect under the baseline contagion intensity $\beta = 1.5\beta_c^{ref}$, and the vertical dashed line marks the benchmark delay $T = 5$. Figure 4b compares the delay effect under different contagion intensity levels

The same finite-size BA fixed-point framework also implies that stronger immunization and recovery capacity reduce the long-run infected density. When governance capacity is sufficiently high, the fixed contagion intensity may fall below the corresponding threshold, and the system returns to the risk-free steady state. This reinforces the interpretation that ex ante immunization and ex post recovery improve resilience by raising the stability boundary and reducing persistent credit-risk contagion.

5. Robustness and validation

5.1 *Node-level Monte Carlo validation*

The preceding numerical analysis is based on a degree-based mean-field approximation, which provides tractable threshold and steady-state expressions while retaining network heterogeneity through the degree distribution and degree-weighted exposure terms. To examine whether the main dynamic patterns are preserved at the node level, this subsection conducts Monte Carlo simulations on finite-size BA networks. The purpose of this exercise is validation rather than replacement of the analytical framework. Specifically, the node-level simulations compare aggregate infected-density paths with the mean-field benchmark and examine whether the threshold-type transition remains visible under stochastic contagion dynamics.

The validation is conducted on finite-size BA networks with $N = 1000$ and $m = 5$, using the same benchmark governance, exposure, and delay parameters as in the main numerical analysis. This design keeps the comparison focused on the difference between the degree-based mean-field approximation and node-level stochastic propagation. The contagion intensity is expressed as a multiple of the finite-size BA threshold, $\beta / \beta_c^{BA,0}(N)$, so that subcritical, near-critical, and supercritical regimes can be examined under a common scale. For each parameter setting, $M = 200$ Monte Carlo runs are performed, and the reported node-level infected-density paths are averages across these runs.

Figure 5 reports the node-level Monte Carlo validation. The purpose of this exercise is not to replace the degree-based mean-field model, but to examine whether its main dynamic implications remain visible when contagion is simulated on finite stochastic networks. This is important because the analytical framework aggregates firms by degree class, whereas node-level simulations preserve realization-specific network links, initial shocks, and stochastic state transitions.

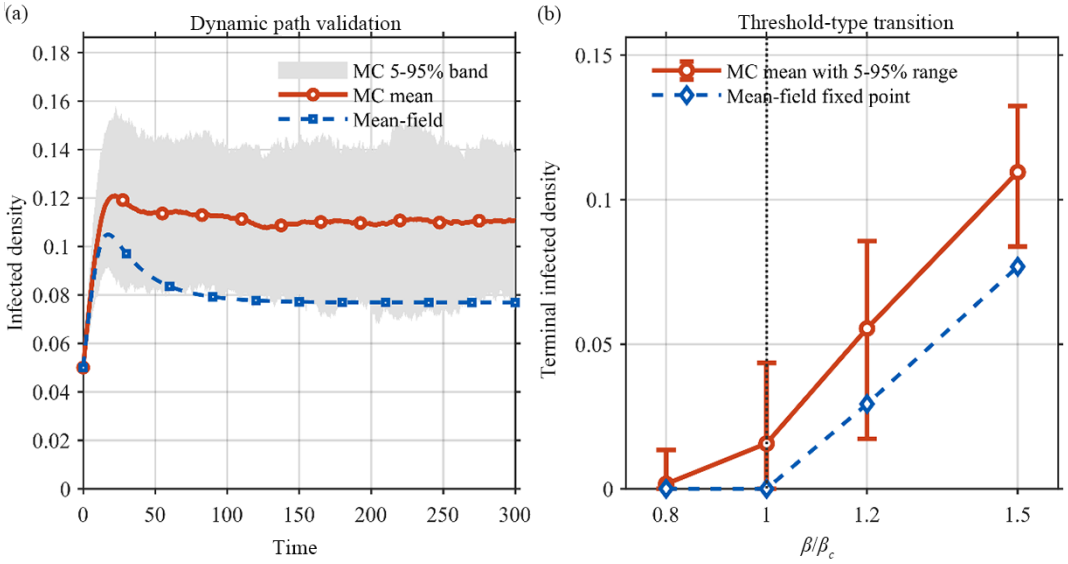


Figure 5. Node-level Monte Carlo validation under the finite-size BA network. The figure compares node-level Monte Carlo simulations with the degree-based mean-field benchmark. The simulations use finite-size BA networks with $N = 1000$ and $m = 5$, and the governance, exposure, and delay parameters are kept at their benchmark values. Figure 5a compares the Monte Carlo average infected-density path with the mean-field path under $\beta = 1.5\beta_c$, where $\beta_c = \beta_c^{BA,0}(N)$. The shaded band reports the 5th–95th percentile range across $M = 200$ Monte Carlo runs. Figure 5b reports the terminal infected density across selected values of β/β_c, with the vertical reference line marking the threshold

Figure 5a compares the aggregate infected-density path from Monte Carlo simulations with the degree-based mean-field benchmark under $\beta = 1.5\beta_c$. The Monte Carlo average path follows the same qualitative pattern as the mean-field path: the infected density rises after the initial credit-risk shock, then declines and converges to a persistent positive level. The node-level simulations produce a somewhat higher long-run infected density than the mean-field benchmark. This difference is expected, because finite stochastic networks preserve local propagation paths, realization-specific connectivity, and random transition events that are averaged out in the mean-field approximation. The 5th–95th percentile band further shows non-negligible dispersion across Monte Carlo runs, reflecting the stochastic nature of node-level contagion.

Figure 5b examines whether the threshold-type transition remains visible at the node level. The terminal infected density increases with β/β_c. Subcritical and near-critical cases generate relatively low terminal infection levels, whereas supercritical cases produce higher persistent infection. The transition in the Monte Carlo simulations is smoother than the mean-field fixed point because the simulations are conducted on finite stochastic networks over a finite time horizon. Nevertheless, the upward shift in terminal infected density around and above the threshold is consistent with the threshold mechanism implied by the degree-based mean-field model.

These results support the use of the degree-based mean-field approximation as the main analytical framework. The node-level simulations are not intended to provide an exact finite-network proof of the mean-field threshold. Rather, they show that the threshold-type transition remains visible when realized links, stochastic initial shocks, and random transition histories are explicitly simulated. Exact agreement is not expected because the mean-field model averages over degree classes, whereas the Monte Carlo simulations preserve realized links and stochastic transition histories. Nevertheless, the key qualitative implications are preserved: infection rises after the initial shock, persistent infection emerges in the supercritical region, and terminal infection levels increase with β/β_c. The degree-based mean-field framework should therefore be viewed as a degree-class closure rather than a fully homogeneous approximation.

5.2 *Degree-dependent asset connectedness robustness*

The benchmark simulations use the constant-exposure specification $\eta_k = \eta_0$ to keep the main mechanism transparent. However, in financial networks, highly connected firms may also have stronger asset connectedness because they are

more likely to maintain multiple credit, trade, and balance-sheet links. To examine whether the main results depend on the constant-exposure benchmark, this subsection allows asset connectedness to vary across degree classes.

Specifically, we consider the following degree-dependent specification:

$$\eta_k = min\left\{\eta_{\max}, \eta_0\left(\frac{k}{\langle k\rangle_{BA,N}}\right)^{\chi}\right\},$$

where χ measures the strength of the association between node degree and asset connectedness. The case $\chi = 0$ corresponds to the constant-exposure benchmark. A larger χ means that high-degree firms carry stronger asset connectedness. The upper bound $\eta_{\max}$ is imposed to keep η_k within an economically meaningful range. For each value of χ, the degree-weighted asset-connectedness term is recalculated as

$$M_{\eta,N}^{BA} = \sum_{k=m}^{k_{\max}(N)} k^2 P_{BA,N}(k)\eta_k.$$

The corresponding finite-size BA threshold is then computed using the recalculated $M_{\eta,N}^{BA}$. The contagion intensity is fixed relative to the constant-exposure benchmark threshold and is not recalibrated when χ changes. This design isolates the effect of degree-dependent asset connectedness.

Figure 6 shows that the main conclusions are robust to degree-dependent asset connectedness. Figure 6a shows that the contagion threshold declines as χ increases. This pattern is consistent with the threshold expression. When asset connectedness becomes more concentrated among high-degree firms, $M_{\eta,N}^{BA}$ increases because η_k receives greater weight in high-k degree classes. Since the threshold is inversely related to $M_{\eta,N}^{BA}$, stronger degree-dependent asset connectedness lowers the stability boundary of the associated credit network.

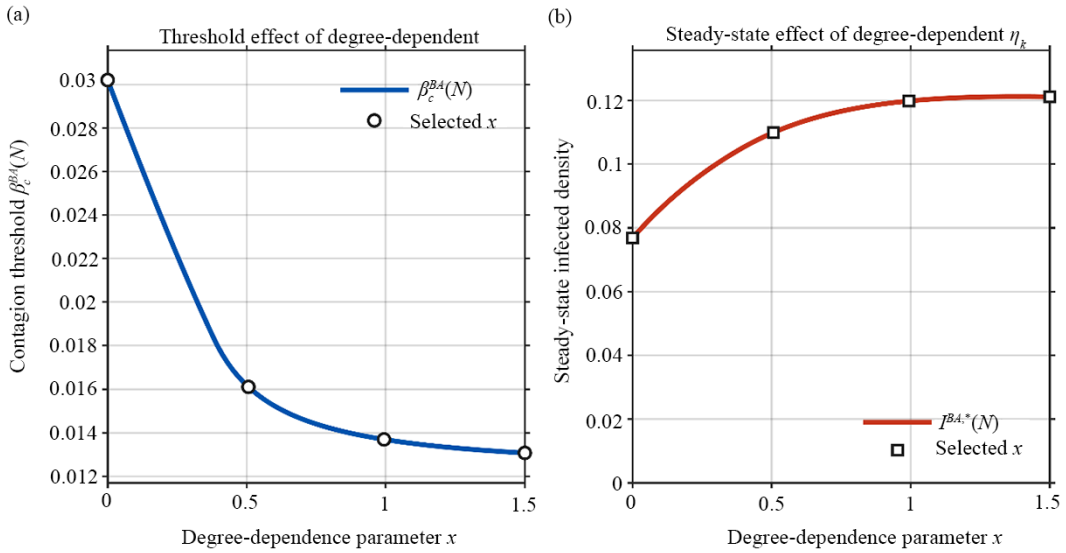


Figure 6. Robustness to degree-dependent asset connectedness under the finite-size BA network. The figure reports robustness results when asset connectedness varies across degree classes according to $\eta_k = \min\{\eta_{\max}, \eta_0(k/\langle k\rangle_{BA,N})^{\chi}\}$. The case $\chi = 0$ corresponds to the constant-exposure benchmark. Figure 6a reports the contagion threshold $\beta_c^{BA}(N)$. Figure 6b reports the steady-state infected density $I^{BA,*}(N)$ under a fixed contagion intensity set relative to the constant-exposure benchmark threshold

Figure 6b reports the corresponding steady-state infected density. Under the fixed contagion intensity used in the simulation, $I^{BA,*}(N)$ increases as χ rises. This means that, once highly connected firms are also more strongly linked through asset exposure, a given contagion intensity generates a higher long-run infection level. The curve becomes flatter at higher values of χ, reflecting the upper bound imposed on η_k. This cap prevents asset connectedness from becoming unrealistically large and keeps the robustness exercise within a plausible parameter range.

These results indicate that the constant-exposure benchmark does not drive the main findings. If high-degree firms also carry stronger asset connectedness, the contagion threshold becomes lower and the steady-state infected density becomes higher. Thus, allowing η_k to vary by degree strengthens rather than weakens the paper's central mechanism: network heterogeneity and asset-exposure heterogeneity jointly increase systemic vulnerability.

5.3 *Network-size robustness*

Although the benchmark simulations use $N = 1000$, the contagion threshold may vary with network size because the finite-size BA degree distribution and its degree moments change with N. To examine whether the main results are driven by a single network-size choice, we evaluate the threshold under alternative finite-size BA networks. For each value of N, the normalized degree distribution $P_{BA,N}(k)$, the first degree moment $\langle k\rangle_{BA,N}$, and the second degree moment $\langle k^2\rangle_{BA,N}$ are recalculated before computing the corresponding threshold.

The network-size results are reported in Figure 2. Figure 2c shows that $\beta_c^{BA,0}(N)$ declines as N increases under the selected delay levels. Figure 2d provides the structural explanation: the ratio $\langle k\rangle_{BA,N}/\langle k^2\rangle_{BA,N}$ decreases with N, indicating that the second degree moment becomes more influential in larger finite-size BA networks. Since the threshold is proportional to this structural ratio under the constant-exposure benchmark, larger BA networks exhibit lower contagion thresholds.

This robustness check shows that the main threshold mechanism is not an artifact of the benchmark network size. The decline in $\beta_c^{BA,0}(N)$ across larger finite-size BA networks is consistent with the paper's central mechanism: stronger degree heterogeneity lowers the stability boundary and makes persistent credit-risk contagion easier to sustain. Therefore, the benchmark choice of $N = 1000$ does not drive the threshold result.

6. Conclusion

This paper develops a delay-embedded D-SIRS model to study inter-firm associated credit-risk contagion on complex networks. Combining a degree-based mean-field framework with threshold analysis, numerical simulations, and node-level Monte Carlo validation, the paper shows that associated credit risk follows a clear regime-switching logic. When contagion intensity remains below the critical threshold, local shocks die out and the system converges to a risk-free state. Once the threshold is crossed, credit stress can become persistent and the system may move toward an endemic-risk regime. The stability boundary is shaped by three interacting forces: network topology, exposure heterogeneity, and governance capacity. Degree-weighted asset connectedness, longer response delays, faster immunity waning, larger finite-size BA networks, and stronger degree heterogeneity lower the threshold and increase persistent-risk exposure. By contrast, stronger immunization and recovery raise the threshold and improve systemic resilience. The node-level Monte Carlo results further show that this threshold-type transition remains visible under stochastic finite-network propagation.

These results should be interpreted as mechanism-based evidence rather than as directly estimated policy effects. The model identifies how prevention, recovery, delay reduction, and exposure restructuring affect the stability boundary, but it does not estimate their magnitudes for a specific financial system. The findings nevertheless offer several implications for the governance of associated credit risk. First, structural governance should limit highly concentrated asset linkages and reduce strongly contagious connections among core firms, especially when high-degree firms also carry large direct asset exposures. Second, timely intervention is critical. Delays in risk identification, information reporting, intervention, or recovery lower the stability boundary and allow local stress to accumulate within the response window. Third, prevention and resolution should be coordinated rather than treated as substitutes. Ex ante immunization through early warning, exposure reduction, and preventive credit control can reduce the likelihood that vulnerable firms enter distress, while ex

post recovery through liquidity support, debt restructuring, and guarantee resolution can shorten the persistence of realized stress. Effective governance therefore depends not on intensifying a single policy tool, but on matching policy instruments to intervention timing and to the structural constraints of the network.

Several limitations should be acknowledged. This study is best viewed as a mechanism-based theoretical analysis rather than an episode-specific empirical calibration. The parameters are used for analytical and numerical exploration and have not yet been externally estimated using firm-level exposure, linkage, or transaction data. Future work could use inter-firm credit linkages, supply-chain transactions, guarantee networks, or financial connectedness data to estimate the key parameters and examine the model's threshold implications in observed financial networks. Further extensions could also incorporate heterogeneous delays, time-varying network structures, multilayer exposures, and dynamic regulatory responses.

Author contributions

Xiaogang Liu: Writing—original draft, Software, Methodology. Jinmian Han: Methodology, Conceptualization. Dongqi Yue: Writing—original draft, Software, Formal analysis. Huaigu Tian: Software, Methodology.

Funding

This research was supported by the Natural Science Basic Research Program of Shaanxi (2024JC-YBMS-068) and the Scientific Research Program Funded by Shaanxi Provincial Education Department (25JK0712).

Acknowledgement

The authors are grateful to their colleagues and peers for valuable discussions and insightful comments on complex network modeling, contagion dynamics, and numerical simulation methods throughout this study.

Data availability statement

No empirical data were used. All numerical results were generated from the model and parameter settings reported in the paper.

Conflict of interest

The authors declare no competing financial interest.

References

[1] Acemoglu D, Carvalho VM, Ozdaglar A, Tahbaz-Salehi A. The network origins of aggregate fluctuations. *Econometrica*. 2012; 80(5): 1977–2016. Available from: https://doi.org/10.3982/ECTA9623.

[2] Carvalho VM, Nirei M, Saito YU, Tahbaz-Salehi A. Supply chain disruptions: Evidence from the Great East Japan Earthquake. *The Quarterly Journal of Economics*. 2021; 136(2): 1255–1321. Available from: https://doi.org/10.1093/qje/qjaa044.

[3] Acemoglu D, Tahbaz-Salehi A. The macroeconomics of supply chain disruptions. *The Review of Economic Studies*. 2025; 92(2): 656–695. Available from: https://doi.org/10.1093/restud/rdae038.

[4] Allen F, Gale D. Financial contagion. *Journal of Political Economy*. 2000; 108(1): 1–33. Available from: https://doi.org/10.1086/262109.

[5] Cifuentes R, Ferrucci G, Shin HS. Liquidity risk and contagion. *Journal of the European Economic Association*. 2005; 3(2–3): 556–566. Available from: https://doi.org/10.1162/jeea.2005.3.2-3.556.

[6] Gai P, Kapadia S. Contagion in financial networks. *Proceedings of the Royal Society A*. 2010; 466(2120): 2401–2423. Available from: https://doi.org/10.1098/rspa.2009.0410.

[7] Elliott M, Golub B, Jackson MO. Financial networks and contagion. *American Economic Review*. 2014; 104(10): 3115–3153. Available from: https://doi.org/10.1257/aer.104.10.3115.

[8] Acemoglu D, Ozdaglar A, Tahbaz-Salehi A. Systemic risk and stability in financial networks. *American Economic Review*. 2015; 105(2): 564–608. Available from: https://doi.org/10.1257/aer.20130456.

[9] Tipsri S, Chinviriyasit W. The effect of time delay on the dynamics of an SEIR model with nonlinear incidence. *Chaos, Solitons & Fractals*. 2015; 75: 153–172. Available from: https://doi.org/10.1016/j.chaos.2015.02.017.

[10] Luo H, Tan J. Risk contagion of net international short-term capital flows: A volatility spillover network perspective. *Finance Research Letters*. 2025; 84: 107730. Available from: https://doi.org/10.1016/j.frl.2025.107730.

[11] Watts DJ, Strogatz SH. Collective dynamics of "small-world" networks. *Nature*. 1998; 393(6684): 440–442. Available from: https://doi.org/10.1038/30918.

[12] Barabási AL, Albert R. Emergence of scaling in random networks. *Science*. 1999; 286(5439): 509–512. Available from: https://doi.org/10.1126/science.286.5439.509.

[13] Newman MEJ. The structure and function of complex networks. *SIAM Review*. 2003; 45(2): 167–256. Available from: https://doi.org/10.1137/S003614450342480.

[14] Buldyrev SV, Parshani R, Paul G, Stanley HE, Havlin S. Catastrophic cascade of failures in interdependent networks. *Nature*. 2010; 464(7291): 1025–1028. Available from: https://doi.org/10.1038/nature08932.

[15] Haldane AG, May RM. Systemic risk in banking ecosystems. *Nature*. 2011; 469(7330): 351–355. Available from: https://doi.org/10.1038/nature09659.

[16] Glasserman P, Young HP. Contagion in financial networks. *Journal of Economic Literature*. 2016; 54(3): 779–831. Available from: https://doi.org/10.1257/jel.20151228.

[17] Ma W, Song M, Takeuchi Y. Global stability of an SIR epidemic model with time delay. *Applied Mathematics Letters*. 2004; 17: 1141–1145. Available from: https://doi.org/10.1016/j.aml.2003.11.005.

[18] Liu Q, Deng C, Sun M. The analysis of an epidemic model with time delay on scale-free networks. *Physica A*. 2014; 410: 79–87. Available from: https://doi.org/10.1016/j.physa.2014.05.010.

[19] Sun M, Liu Q. An SIS epidemic model with time delay and stochastic perturbation on heterogeneous networks. *Mathematical Biosciences and Engineering*. 2021; 18(5): 6790–6805. Available from: https://doi.org/10.3934/mbe.2021337.

[20] Liu J. Bifurcation analysis for a delayed SEIR epidemic model with saturated incidence and saturated treatment function. *Journal of Biological Dynamics*. 2019; 13(1): 461–480. Available from: https://doi.org/10.1080/17513758.2019.1631965.

[21] Battiston S, Puliga M, Kaushik R, Tasca P, Caldarelli G. DebtRank: Too central to fail? Financial networks, the FED and systemic risk. *Scientific Reports*. 2012; 2: 541. Available from: https://doi.org/10.1038/srep00541.

[22] Diebold FX, Yilmaz K. On the network topology of variance decompositions: Measuring the connectedness of financial firms. *Journal of Econometrics*. 2014; 182(1): 119–134. Available from: https://doi.org/10.1016/j.jeconom.2014.04.012.

[23] Yang R, Tian H, Wang Z, Wang W, Zhang Y. Dynamical analysis and synchronization of complex network dynamic systems under continuous-time. *Symmetry*. 2024; 16(6): 687. Available from: https://doi.org/10.3390/sym16060687.

[24] Fiori AM, Porro F. A compositional analysis of systemic risk in European financial institutions. *Annals of Finance*. 2023; 19: 325–354. Available from: https://doi.org/10.1007/s10436-023-00427-0.

[25] Zhao Q, Wang Z, Song Y. Systematic research on multi-dimensional and multiple correlation contagion networks of extreme risk in China's banking industry. *Computational Economics*. 2024; 64: 1137–1162. Available from: https://doi.org/10.1007/s10614-023-10474-4.

[26] Baruník J, Caldarelli G, May RM, Roukny T, Ellington M. Persistence in financial connectedness and systemic risk. *European Journal of Operational Research*. 2024; 314(1): 393–407. Available from: https://doi.org/10.1016/j.ejor.2023.11.023.

[27] Camera G, Gioffré A. Financial contagion and financial lockdowns. *Journal of Economic Behavior & Organization*. 2024; 218: 613–633. Available from: https://doi.org/10.1016/j.jebo.2024.01.002.

[28] Cooke KL, van den Driessche P. Analysis of an SEIRS epidemic model with two delays. *Journal of Mathematical Biology*. 1996; 35(2): 240–260. Available from: https://doi.org/10.1007/s002850050051.

[29] Xu XJ, Chen G. The SIS model with time delay on complex networks. *International Journal of Bifurcation and Chaos*. 2009; 19(2): 623–628. Available from: https://doi.org/10.1142/S021812740902324X.

[30] Xu R, Wang Z, Zhang F. Global stability and Hopf bifurcations of an SEIR epidemiological model with logistic growth and time delay. *Applied Mathematics and Computation*. 2015; 269: 332–342. Available from: https://doi.org/10.1016/j.amc.2015.07.084.

[31] Pastor-Satorras R, Vespignani A. Epidemic dynamics and endemic states in complex networks. *Physical Review E*. 2001; 63(6): 066117. Available from: https://doi.org/10.1103/PhysRevE.63.066117.